Plant, Cell and Environment (1998) **21,** 347–359

Limitation of plant water use by rhizosphere and xylem conductance: results from a model

J. S. SPERRY,[1] F. R. ADLER,[2] G. S. CAMPBELL[3] & J. P. COMSTOCK[4]

[1]*Department of Botany, Box 90338, Duke University, Durham, NC 27708,* [2]*Department of Biology, University of Utah, Salt Lake City, UT 84112,* [3]*Department of Crop and Soil Science, Washington State University, Pullman, WA 99164–6420, and* [4]*Boyce Thompson Institute for Plant Research, Tower Road, Ithaca, NY 14853, USA*

ABSTRACT

Hydraulic conductivity (K) in the soil and xylem declines as water potential (Ψ) declines. This results in a maximum rate of steady-state transpiration (E_{crit}) and corresponding minimum leaf Ψ (Ψ_{crit}) at which K has approached zero somewhere in the soil–leaf continuum. Exceeding these limits causes water transport to cease. A model determined whether the point of hydraulic failure (where $K = 0$) occurred in the rhizosphere or xylem components of the continuum. Below a threshold of root:leaf area (A_R:A_L), the loss of rhizosphere K limited E_{crit} and Ψ_{crit}. Above the threshold, loss of xylem K from cavitation was limiting. The A_R:A_L threshold ranged from > 40 for coarse soils and/or cavitation-resistant xylem to < 0·20 in fine soils and/or cavitation-susceptible xylem. Comparison of model results with drought experiments in sunflower and water birch indicated that stomatal regulation of E reflected the species' hydraulic potential for extracting soil water, and that the more sensitive stomatal response of water birch to drought was necessary to avoid hydraulic failure. The results suggest that plants should be xylem-limited and near their A_R:A_L threshold. Corollary predictions are (1) within a soil type the A_R:A_L should increase with increasing cavitation resistance and drought tolerance, and (2) across soil types from fine to coarse the A_R:A_L should increase and maximum cavitation resistance should decrease.

Key-words: drought responses; hydraulic conductance; rhizosphere conductance; root–shoot ratio; soil–root interface; water relations; water transport; xylem cavitation.

INTRODUCTION

As postulated by the cohesion-tension theory, the flow of water from soil to leaf represents a 'tug-of-war' on a hydraulic rope. If the hydraulic continuum breaks, the plant cannot access atmospheric CO_2 without desiccating to death. There are two weak spots in the continuum: at the rhizosphere where steep water potential gradients may create dry non-conductive zones (Newman 1969), and in the xylem where cavitation can eliminate water transport (Zimmermann 1983). While earlier studies have considered the limitation of water uptake by one or the other of these processes (Newman 1969; Bristow, Campbell & Calissendorff 1984; Tyree & Sperry 1988), it is an open question how rhizosphere and xylem properties interact to limit water uptake. In this paper, we answer this question with a model.

Correspondence: J. S. Sperry. Fax: 919 6607293; e-mail: jsperry@duke.edu

The theory of hydraulic limits on water uptake begins with Darcy's law, which can be applied to steady-state flow through the soil–plant hydraulic continuum:

$$E = -K\, d\Psi/dx, \quad (1)$$

where E is the transpiration rate (per leaf area), $d\Psi/dx$ is the water potential gradient driving flow, and K is the hydraulic conductivity expressed per leaf area (Table 1 lists symbols, definitions, and units). Figure 1 shows the steady-state relationship between E and leaf Ψ for a constant bulk soil Ψ (Ψ_s = the Ψ intercept). If K is a constant, E is directly proportional to the decrease in leaf Ψ and there is no hydraulic limit to E or leaf Ψ (dashed line 4 in Fig. 1).

Hydraulic limits arise because K is not constant, but instead decreases in xylem and soil as a function of decreasing Ψ. In the xylem, the decline in K is caused by cavitation, and the K (Ψ) function is described by a 'vulnerability curve' (e.g. Fig. 3). In the soil, the decrease in K occurs by the same mechanism causing cavitation in xylem: the displacement of water-filled pore space by air as capillary forces fail (Hillel 1980; Pockman, Sperry & O'Leary 1995). The $K(\Psi)$ function for soil depends largely on soil texture, with more sensitive functions for coarser soils (Hillel 1980).

When Ψ-dependent K is incorporated into Darcy's law, there is no longer a directly proportional relationship between E and Ψ (Fig. 1, curves 1–3). Instead, increases in E are associated with progressively disproportionate decreases in Ψ because of declining K. The E reaches a maximum (E_{crit}) at the corresponding minimum leaf Ψ (Ψ_{crit}). At these critical values, K (Ψ) has approached zero somewhere in the hydraulic continuum (Appendix). As Ψ_s decreases, E_{crit} declines (Fig. 1, compare curves 1–3). When $\Psi_s = \Psi_{crit}$, the plant cannot transport water.

If stomata allow E to exceed E_{crit} long enough for steady-state conditions to develop, the positive feedback

Symbol	Definition	Units
A_L	leaf area	m^2
A_R	absorbing root area	m^2
a	fraction of plant volume	–
b	soil texture parameter	–
c	Weibull function parameter	–
C	capacitance (per A_L)	mmol MPa^{-1} m^{-2}
d	Weibull function parameter	–
E	transpiration rate (per A_L)	mmol s^{-1} m^{-2}
E_{crit}	maximum transpiration rate	mmol s^{-1} m^{-2}
F	flux balance	mmol s^{-1}
i	node number	–
K	hydraulic conductivity	mmol s^{-1} MPa^{-1} m^{-1}
k	hydraulic conductance	mmol s^{-1} MPa^{-1}
K_s	maximum soil conductivity	mmol s^{-1} MPa^{-1} m^{-1}
k_s	maximum element conductance	mmol s^{-1} MPa^{-1}
L	root length density	m m^{-3}
r	radius of soil node	m
W	water content	mmol m^{-3}
W_s	saturated water content	mmol m^{-3}
X	soil conductance factor	m
Greek symbols		
Φ	matric flux potential	mmol s^{-1}
Ψ	water potential	MPa
Ψ_e	air entry potential, soil	MPa
Ψ_s	soil water potential	MPa
Ψ_{crit}	critical water potential	MPa

Table 1. List of major symbols and their definitions. Units are those used in equations. Values cited in text or figures may have different units

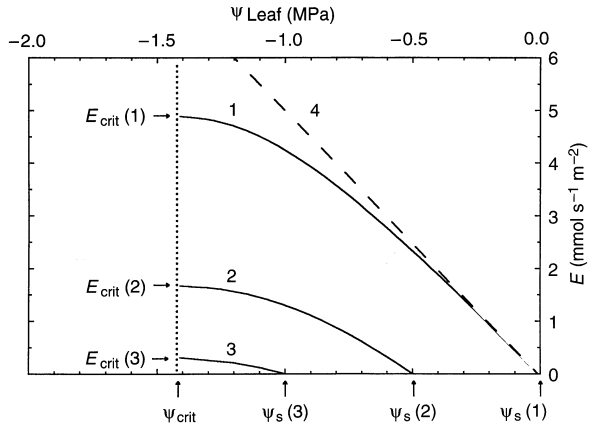

Figure 1. Definition of hydraulic limits. The transpiration rate (E) versus Ψ leaf is based on the model solution of Darcy's law. Solid curves 1–3 are for water birch xylem (Fig. 3) in loam soil (Table 2), at three soil Ψ values (Ψ_s). Maximum transpiration rate is E_{crit}, and is dependent on Ψ_s. The leaf Ψ at E_{crit} is Ψ_{crit} (vertical dotted line). The Ψ_{crit} is also the lowest Ψ_s permitting water uptake. The dashed line (4) represents constant hydraulic conductance in the continuum, in which case there are no hydraulic limits.

between decreasing K and Ψ becomes unstable: a phenomenon dubbed 'runaway cavitation' when it occurs in xylem (Tyree & Sperry 1988). Runaway cavitation breaks the hydraulic rope and eliminates water transport by driving K to zero. A model by Tyree & Sperry (1988) predicted an E_{crit} that was only slightly greater than actual maximum E in four diverse tree species, suggesting stomatal regulation of E was adaptive in avoiding hydraulic failure of the xylem. The gas exchange capacity of plants may have hydraulic constraints.

The Tyree and Sperry model, however, did not incorporate the K (Ψ) relationship for the soil. Transpiration-driven decreases in Ψ soil are accentuated in the rhizosphere because of the cylindrical geometry of water uptake (Cowan 1965; Newman 1969; Bristow, Campbell & Calissendorff 1984), and 'runaway cavitation' can potentially occur at the soil–root interface. Rhizosphere limitations should be especially important for coarse soils and plants with less absorbing root area relative to their transpiring leaf area (Newman 1969). Although variable rhizosphere conductance has been incorporated in water uptake models (Cowan 1965; Bristow *et al*. 1984), none have incorporated variable xylem conductance. It is not clear whether below-ground hydraulic constraints are more or less important than those of the xylem.

The model presented in this paper shows how three causal factors – (1) cavitation resistance, (2) root:leaf area ratio (A_R:A_L), and (3) soil type (specifically, soil texture) – interact to set hydraulic limits on water transport. The analysis of cavitation resistance includes the influence of root xylem, which is more vulnerable than canopy xylem in many species (Sperry & Saliendra 1994; Alder, Sperry & Pockman 1996; Hacke & Sauter 1996; Mencuccini & Comstock 1997). The purpose of the model is to obtain a

better understanding of biophysical limits on water uptake and their relevance to physiological responses of plants to water availability.

THE MODEL

Flux balance equations and hydraulic conductance functions

The model uses the standard finite-difference approach to solving Darcy's law for the soil–plant hydraulic pathway (Campbell 1985). The soil–leaf continuum was divided into 'nodes' and connecting 'elements' (Fig. 2; see below). The soil elements defined a cylindrical rhizosphere adjacent to the absorbing roots. For each node i (ascending from $i = 1$ at the leaves, Fig. 2), we wrote the flux balance, or Richards', equation (Ross & Bristow 1990) in which the difference in flux of water leaving versus entering node i equals the change in water content at node i ($\Delta W = W_{t=1} - W_{t=2}$) over time step Δt ($t_2 - t_1$). These equations assume the driving forces ($\Delta\Psi_i = \Psi_{i+1} - \Psi_i$) are differences in water pressure (i.e. osmotic effects are ignored):

$$F_i(\Psi_i, \Psi_{i+1}, \Psi_{i-1}) = k_{i-1}\Delta\Psi_{i-1} - k_i\Delta\Psi_i - \Delta W_i/\Delta t, \quad (2)$$

where k_i is the hydraulic conductance of the element subtending node i, and F_i is the mass balance for node i which equals zero for the correct values of Ψ_i, Ψ_{i+1}, and Ψ_{i-1}. Note that in formulating Eqn 2, hydraulic *conductivity* (K, Eqn 1), which is a length- and/or area-independent parameter, is converted to *conductance* (k) which incorporates the specific geometry of element i (Table 1).

The water content (W, moles of water per volume of tissue or soil) and hydraulic conductance in Eqn 2 are both functions of Ψ. In the soil we used Campbell's (1985) equation,

$$W_i = W_s(\Psi_e/\Psi_i)^{-1/b} \quad (3)$$

where W_s is the water content at maximum hydration where $\Psi_i = \Psi_e$, and b is a soil-texture parameter that increases with finer texture (Table 2). The value for Ψ_e in soil was taken as the 'air-entry' value, which is also a function of soil texture (Table 2; Campbell 1985). In the plant, ΔW_i for Eqn 2 was calculated as:

$$\Delta W_i = a_i\Delta\Psi_i A_L C, \quad (4)$$

where C is the whole-plant capacitance or change in water content per change in Ψ per leaf area, A_L is the leaf area, $\Delta\Psi_i$ is the change in Ψ at node i over the time step, and a_i is the fraction of the total plant volume with which node i exchanges water.

The hydraulic conductance function for the rhizosphere elements was taken from Campbell (1985):

$$k_i = X_i K_s(\Psi_e/\Psi_i)^{(2+3/b)}, \quad (5)$$

where K_s is the maximum soil hydraulic conductivity at saturation (at $\Psi_i = \Psi_e$), b is the soil texture parameter in Eqn 3, and X_i is a factor that converts hydraulic conductivity to hydraulic conductance. We assumed a cylindrical geometry for water uptake by roots so that nodes were at progressively greater radial distances from the root centre (Fig. 2). The 'conductance factor' for the cylindrical flow geometry of the rhizosphere elements is:

$$X_i = 2\pi l \ln^{-1}(r_{i+1}/r_i), \quad (6)$$

where l is the total length of absorbing roots, and r_i is the radius of node i (Campbell 1985).

We used a log transformation (Passioura & Cowan 1968) to set rhizosphere nodes exponentially closer together nearer to the root where Ψ gradients are largest. This transformation equates to:

$$r_i = r_s(r_{max}/r_s)^{[(i-s)/m]}, \quad (7)$$

where r_i is the radius of node i, r_s is the radius of the root surface, r_{max} is the radius of the outermost rhizosphere node, s is the node number of the root surface, and m is the number

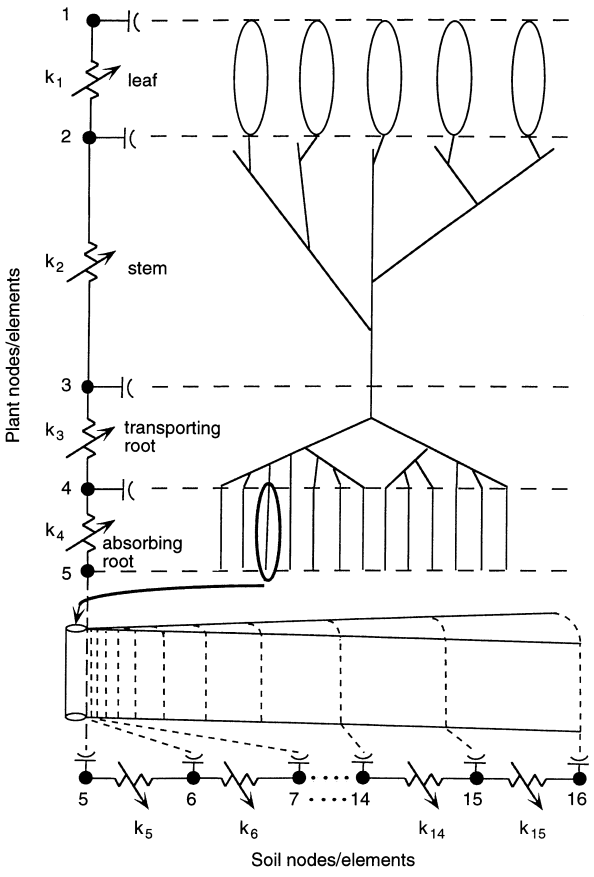

Figure 2. Model organization showing division of the soil–plant hydraulic continuum into 16 nodes and 15 elements. Element conductance is symbolized as variable electrical resistance. Nodes exchange water with a volume of plant or soil. Shoot and root branching was represented by the series conductance of hydraulically equivalent units (k_1: leaves, k_2: shoots, k_3: transporting roots, k_4: absorbing roots). Soil node spacing was set by a log transformation of the distance from the root surface to the outermost soil node (Eqn 7). Roots were assumed to exhibit uniform spacing in a defined soil volume. Solution of Eqn 13 gave Ψ of nodes 1–16 at controlled values of flux from node 1 ($= E A_L$).

Type	*GMD* (mm)	*GSD*	*b*	Ψ_s (kPa)	K_s (mol s^{-1} MPa^{-1} m^{-1})
Sand	0·7	5	2·20	–0·60	130·8
Loamy sand	0·4	5·3	2·64	–0·79	75·1
Sandy loam	0·3	7·4	3·31	–0·91	53·2
Silt loam	0·1	6·1	4·38	–1·58	12·1
Fritted clay	–	–	5·12	–1·68	11·1
Loam	0·07	14	6·58	–1·88	12·7
Clay	0·007	15	14·95	–5·98	1·69

Table 2. Soil parameters. GMD, geometric mean particle diameter; GSD, geometric standard deviation of particle size; Ψ_e, air entry potential ($\Psi_e = -0{\cdot}5\ GMD^{-0{\cdot}5}$; Campbell 1985); *b*, soil texture parameter ($b = -2\ \Psi_e + 0{\cdot}2\ GSD$, Campbell 1985); K_s, saturated (maximum) hydraulic conductivity. All soils were assumed to have a bulk density of 1·3 Mg m^{-3}

of rhizosphere elements. We assumed the absorbing roots were uniformly aligned in the soil volume such that their associated soil cylinders exhibited closest packing in the soil space. Under these conditions, r_{max} is related to root length density of absorbing roots (*L*; length per soil volume):

$$r_{max} = (\pi L)^{-0{\cdot}5} \tag{8}$$

(Campbell 1985).

The hydraulic conductance function for the plant elements was based on a Weibull model fit (Rawlings & Cure 1985; Neufeld *et al*. 1992) to empirical vulnerability curves (Fig. 3). The Weibull equation includes two curve-fitting parameters (*d* and *c*):

$$k_i = k_s\, e^{-(-\Psi_i/d)^c}, \tag{9}$$

where k_i is the hydraulic conductance of element *i*, Ψ_i is the xylem pressure at node *i* and k_s is the element's maximum conductance in the absence of cavitation. Values for *d* and *c* were obtained using a standard curve-fitting routine. There is no conductance factor in Eqn 9 because k_s was inputted as conductance rather than conductivity.

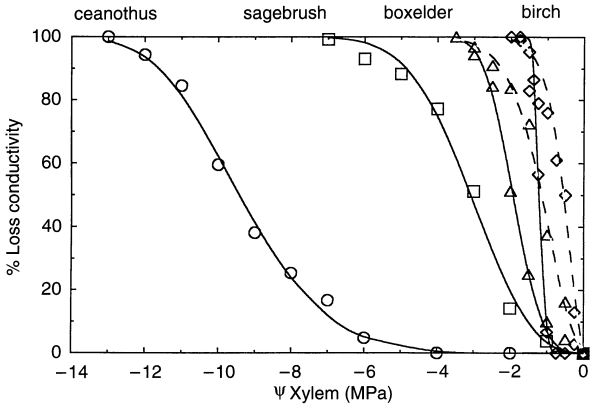

Figure 3. The $K(\Psi)$ functions for plant elements (k_1 to k_4 in Fig. 2) in terms of percentage loss in hydraulic conductivity. Curves show the Weibull function:

$[100\ (1 - e^{-(-\Psi/d)^c})$; Eqn 9] as fitted to xylem cavitation data on stems (solid lines) and roots (dashed lines). Root data were available only for water birch (*Betula occidentalis*) and boxelder (*Acer negundo*). Four xylem types are shown: hoary leaf ceanothus (*Ceanothus crassifolius*, $d = 10{\cdot}05$, $c = 5{\cdot}71$), mountain sagebrush (*Artemisia tridentata* ssp. *vaseyana*, $d = 3{\cdot}54$, $c = 2{\cdot}64$), boxelder (stems: $d = 2{\cdot}15$, $c = 3{\cdot}43$; roots: $d = 1{\cdot}41$, $c = 1{\cdot}78$), and water birch (stems: $d = 1{\cdot}28$, $c = 9{\cdot}53$; roots: $d = 0{\cdot}70$, $c = 1{\cdot}50$).

A preliminary model solved the nodal Richards' equations (Eqn 2) by converting them to ordinary differential equations (for $d\Psi/dt$) and integrating with the Runge-Kutta procedure (Press *et al*. 1989). This proved inordinately time-consuming on the computer because the non-linearity of the *k* functions in the equation required extraordinarily small time steps (< 0·001 s) under wet soil conditions. The present version linearized the Richards' equation using the 'Kirchhoff transform,' an integral transform (Ross & Bristow 1990) that substitutes 'matric flux potential' (Φ) for $\Delta\Psi$ as the driving force for flow (Campbell 1985). Matrix flux potential is the integral of hydraulic conductance from $\Psi = \Psi_i$ to $-\infty$:

$$\Phi_i = \int_{-\infty}^{\Psi_i} k_i(\Psi)\ d\Psi_i. \tag{10}$$

Integrating Eqn 5 for soil element conductance gives:

$$\Phi_i = k_i\ \Psi_i/(-1-3/b). \tag{11}$$

Equation 9, the Weibull function for plant hydraulic conductance, can only be integrated using numeric methods. The equation was converted to the complement of an incomplete gamma function for which a numerical routine was available (Press *et al*. 1989):

$$\Phi_i = k_s\, d/c \int_{z(\Psi_i)}^{z(\infty)} e^{-z}\, z^{(h-1)}\, dz, \tag{12}$$

where $z = (-\Psi_i/d)^c$, and $h = 1/c$.

The Richards' equation (Eqn 2) written in the form of Φ gives:

$$F_i(\Phi_i, \Phi_{i+1}, \Phi_{i-1}) = (\Phi_i - \Phi_{i-1}) - (\Phi_{i+1} - \Phi_i) - (\Delta W_i/\Delta t), \tag{13}$$

which results in element conductance of unity, linearizes the steady flow equation, and allows it to be integrated for each element using practical time steps of 1 h (the default setting). However, the transient flow problem remains non-linear because of the dependence of *W* on Ψ (Eqn 3). To solve the set of $i + 1$ simultaneous equations for $F_i = 0$ at each time step, we used the Newton–Raphson method (Campbell 1985). This routine iteratively adjusts each Ψ_i until $\Sigma_{i=1}^{i=n} |F_i|$ converged on zero (where n = total nodes in model). The model was written in visual basic within the Excel 5·0 spreadsheet application (Microsoft, Inc.).

Discretizing the soil–plant continuum

An important advantage of the Kirchhoff transform (Eqn 13) is that it minimizes the number of nodes required to obtain the steady-state solution of E_{crit} and associated parameters. With the Richards' equation (Eqn 2), E_{crit} estimates converge on the proper solution as the continuum is more finely discretized, and preliminary tests are necessary to determine an acceptable number of nodes. The Kirchhoff transform gives the correct E_{crit} and Ψ_{crit} whether the continuum is represented by 1 or 100 nodes (Appendix), as long as the $k(\Psi)$ function is the same along the flow path. To solve for steady-state E_{crit}, discretizing is only necessary if the $k(\Psi)$ functions change through the continuum, as they do within soil because of the changing conductance factor X_i (Eqns 5 & 6), and within the plant because of possibly different values of d and c for the Weibull function (Eqn 9) along the flow path. We applied the same procedures developed by Ross & Bristow (1990) for applying the Kirchhoff transform to a hydraulic continuum across media with different $k(\Psi)$ and $W(\Psi)$ functions.

We divided the soil–leaf continuum into 16 nodes with 15 connecting elements (Fig. 2). The plant consists of four elements: absorbing roots, transporting roots, stems, and leaves. This allowed us to vary the $k(\Psi)$ function between these compartments if desired. In organizing the plant elements we applied the pipe-model principle (Shinozaki *et al*. 1964) and assumed that the entire hydraulic pathway of a plant from fine roots to evaporating surfaces in the leaf can be represented as a bundle of parallel pipes with equal hydraulic conductance. This means, for example, that the hydraulic conductance from the root collar to the base of the lamina of each leaf is the same, and similarly, the conductance from the base of the lamina to every evaporating surface within the leaf is equivalent. This allowed us to represent the branch system of roots and shoots as a catena of conductance elements and nodes in series, where each element represents the collective (series and parallel) conductance of morphologically equivalent units of the plant (Fig. 2).

Node 1 is the evaporating surface of the leaves, and the subtending conductance (k_1) is the collective conductance of all laminae from the junction with the petiole to the evaporating surface. This flow path includes both xylem and mesophyll components. Node 2 is the petiole–lamina junction, and its subtending conductance (k_2) is the conductance of the xylem of the entire branched stem system, including the petioles. Node 3 is the stem–root junction, and the subtending conductance (k_3) is the conductance of the xylem of the non-absorbing root system. Node 4 is the junction between water-absorbing and non-absorbing roots. The associated conductance (k_4) is the collective conductance of all absorbing roots from the root surface to node 4. Although the flow path in these roots includes both xylem (axial flow) and non-xylem (radial flow) components, we assume that the axial conductance is infinite, and that the water uptake along the length of an absorbing root will be equal. This is a reasonable assumption for the presumably short (≈ 100–200 mm) absorbing zones behind root tips (Steudle 1994).

The rhizosphere was more finely discretized than the plant because of the changing $k(\Psi)$ function with distance from the root surface (Eqn 5). The total rhizosphere volume was divided into 10 nodes. However, tests showed that, under conditions when soil properties were determining E_{crit} and Ψ_{crit} (see 'Results'), as few as three nodes were required for these parameters to be within 2% of their value when using a 50 node model. The reason for such efficient discretizing is the log transformation of the nodes which concentrates them close to the root where the limiting conductance develops (Fig. 2; Eqn 7; Passioura & Cowan 1968).

Associated with each node is a volume of plant tissue or soil with which water was exchanged as nodal pressures changed. The total nodal volume was taken as the adjacent half of the element volume above (downstream from) the node plus the adjacent half of the element volume below (upstream from) the node.

Determination of hydraulic limits

The model was applied to finding E_{crit} and Ψ_{crit} for the continuum. Boundary conditions for the equation set (Eqn 13) were that Ψ at the outermost soil node (i = 16) was set to a constant (Φ_{16} = constant), as was the product $E\,A_L$, which in terms of Eqn 13 was the flux of element i = 0 (substituted for $\Phi_1 - \Phi_0$). Initial conditions were that Ψ at all nodes equalled Ψ_{16}.

The model was verified by setting E to permissible values and testing for flux balance. Under these conditions, fewer than 20 iterations were required to make $\Sigma_{i=1}^{i=16} |F_i| < 0{\cdot}001$ mmol s^{-1}, and cumulative water depletion was within 0·0001% of cumulative transpiration.

To determine E_{crit}, E was incremented in steps of 0·01 mmol s^{-1} m^{-2} from permissible values until $\Sigma_{i=1}^{i=16} |F_i|$ failed to converge on zero after a maximum of 30 iterations. At each increment, the model was run for enough time steps to achieve steady-state flow ($\Sigma_{i=1}^{i=16} |\Delta\Psi_i|/\Delta t < 0{\cdot}001$ MPa h^{-1}). We deliberately set liberal requirements for model failure by adjusting the criteria for flux balance to $\Sigma_{i=1}^{i=16} |F_i| \leq 1$ mmol s^{-1}. The E_{crit} and Ψ_{crit} were the last permissible values before model failure.

The choice of the E increment can influence the E_{crit} and Ψ_{crit} estimates. The prediction of E_{crit} is less sensitive to the E increment than Ψ_{crit} because E approaches E_{crit} in an asymptotic manner, while Ψ decreases abruptly to Ψ_{crit} (Fig. 1). Mathematically, $\Psi_{crit} = -\infty$ because our soil and xylem $K(\Psi)$ functions never reach zero (Eqns 5 & 9; Appendix). Thus, decreasing the E increment caused the model to converge on E_{crit} as Ψ_{crit} became increasingly negative. Our choice of a 0·01 mmol s^{-1} m^{-2} E increment was based on a very conservative estimate of the control sensitivity of stomata. Using this increment, Ψ_{crit} corresponded to > 98% loss of conductance in the limiting element of the continuum (e.g. Fig. 7).

Model parameters

Plant parameters were based largely on data from woody plants.

Secondary parameters

Secondary parameters were held constant for all simulations except when varied for a sensitivity analysis (Table 3).

Maximum hydraulic conductance in the absence of cavitation (k_s in Eqn 9) was equal for all plant elements and scaled with leaf area to give a leaf-specific conductance of 5 mmol s^{-1} MPa^{-1} m^{-2} for the whole plant. This is a typical value for woody plants (Meinzer *et al*. 1995; Saliendra, Sperry & Comstock 1995). The equal conductance for shoot and root systems was a realistic approximation based on measurements in a variety of herbaceous and woody plants (Hellkvist, Richards & Jarvis 1974; Saliendra & Meinzer 1989; Meinzer *et al*. 1992; Sperry & Pockman 1992; Yang & Tyree 1993; Mencuccini & Comstock 1997). While there is evidence that leaves (k_1) and absorbing roots (k_4) have lower conductance than stems and transporting roots (Yang & Tyree 1994; Lopez & Nobel 1991), we set them equal for the sake of simplicity, while conducting a sensitivity analysis to determine the influence of lower conductance in the k_1 and k_4 components.

For plant capacitance (C in Eqn 4), we used the whole-plant, leaf-specific value of 5 mol Mpa^{-1} m^{-2} as estimated for apple trees by Landsberg, Blanchard & Warrit (1976). The choice of a in Eqn 4 divided whole-plant capacitance into leaf (a = 0·4), stem (a = 0·5), transporting root (a = 0·05), and absorbing root (a = 0·05) components. The choice of a was based on biomass fractions of roots, stems, and leaves reported in Givnish (1995) for ≈ 2–6 m trees. The radius of absorbing roots (r_s, in Eqn 7), was 0·1 mm; a typical value for fine roots (Caldwell & Richards 1986).

Primary parameters

Primary parameters were the hypothetical causal factors underlying the hydraulic limits: cavitation resistance, root:leaf area (A_R:A_L), and soil texture.

Four cavitation resistances were chosen to represent the span of known values (Fig. 3) and to establish the d and c values for the $k(\Psi)$ functions of the plant elements (Eqn 9). On the vulnerable end was water birch (*Betula occidentalis*, water birch; Alder *et al*. 1997), representative of obligate riparian trees in the Western United states; on the resistant end was ceanothus (*Ceanothus crassifolius*, hoary leaf ceanothus; Portwood *et al*. 1997), a shrub of the California chaparral. Intermediate vulnerabilities were represented by sagebrush, a mesic-adapted *Artemisia* species (*Artemisia tridentata* ssp. *vaseyana*, mountain sagebrush; K.J. Kolb and J.S. Sperry, in review), and boxelder (*Acer negundo*; U. Hacke and J. S. Sperry, unpublished). All vulnerability data were collected using either the air-injection method (Cochard, Cruiziat & Tyree 1992; Sperry & Saliendra 1994) or the centrifugal force technique (Pockman *et al*. 1995; Alder *et al*. 1997). Data were from stem segments of between 5 and 10 mm diameter. In water birch and boxelder there were additional data from similar-sized root segments (Fig. 3; dashed curves). No data were available for smaller absorbing roots or for leaf xylem.

For sagebrush and ceanothus simulations where we had no root vulnerability data, all four conductance elements were given the same $k(\Psi)$ function. In water birch and boxelder, the two root elements were given the $k(\Psi)$ function for root xylem and the two shoot elements were given the corresponding function for stem xylem. Although the absorbing root and leaf elements include non-xylary flow paths, without any data on the $k(\Psi)$ function we applied the xylem functions by default.

We ran simulations using d and c values that resulted in no cavitation and constant plant k over physiological values of Ψ (d > 50, c > 100). Under these circumstances, the only hydraulic constraint on flux and pressure was in the soil and rhizosphere components of the continuum.

The A_R:A_L was varied from a minimum of 0·24 to 40, a range that includes most measured values (Rendig &

Parameter	Default	Test	%Δ	%ΔE_{crit}	%$\Delta \Psi_{crit}$
Capacitance (mol MPa^{-1} m^{-2})	5	7	+40	0	–3·0
Whole plant k_s/A_R (mmol $s^{-1}MPa^{-1}m^{-2}$)	5	7	+40	+7·1	+1·5
% *R* 3+4	50	70	+40	0	–1·5
% *R* 4	25	35	+40	0	0
% *R* 1	25	35	+40	0	0
Root *l* (m) (r_{max} constant)	3000	4200	+40	+28·6	0
r_{max} (mm) (*l* constant)	5·6	3·4	–40	+10·7	+1·5
k_4	= $k_3(\Psi)$	= k_{s4}	–	+9·6	–1·5

Table 3. Sensitivity analysis. Parameters tested were capacitance, whole-plant k_s/A_L, percentage of plant resistance in root elements 3 and 4 (% *R* 3+4; with equal resistance in elements 3 and 4), percentage of resistance in root element 4 (% *R* 4; with equal resistance for 3+4 and 1+2), percentage of resistance in leaf (% R 1, equal resistance for 3+4 and 1+2), root length (l), distance to outermost soil node (r_{max}), and $k_4 = k_{s4}$ [vs. the same k (Ψ) function as k_3]. Default and test values of each parameter are shown; %Δ = percentage of increase in test value vs. default; %ΔE_{crit} = percentage change in E_{crit}; %$\Delta \Psi_{crit}$ = percentage change Ψ_{crit}. Simulations were for xylem-limited conditions in sagebrush xylem at A_R:A_L = 1·9, soil volume = 0·3 m^3, loam soil, with E_{crit} evaluated at soil Ψ = –2·2 MPa (= 1/3 Ψ_{crit})

Taylor 1989; Glinski & Lipiec 1990; Tyree, Velez & Dalling 1997). This ratio also represented the ratio of hydraulic conductance in rhizosphere versus plant because these were proportional to their respective root and leaf areas. The ratio was varied by changing A_L and/or A_R. The $A_R = 2\pi r_s LV$, where V = soil volume = 0·3 m^3. We varied A_R by changing L. This influenced rhizosphere conductance via changes in l (Eqn 6) and r_{max} (Eqn 7). We also analysed the independent effect of changing l versus r_{max}.

Several soil types were chosen to span the range of textures from clay through loam to coarse sand (Table 2).

Controlled drought experiments

A comprehensive comparison between predictions of E_{crit} and Ψ_{crit} with empirical data awaits experiments designed explicitly for that purpose. However, we were able to make a preliminary comparison using data from controlled drought experiments on sunflower (*Helianthus annuus*) and water birch (*Betula occidentalis*).

Potted plants were grown from seed in fritted clay under well-watered greenhouse conditions until they were ≈ 0·5–1·5 m tall. Cylindrical pots were≈ 0·15 m in diameter and 0·76 m tall, holding ≈ 0·014 m^3 of soil. Values for soil parameter b were obtained by best fit of Eqn 3 to moisture release data for fritted clay (van Bavel, Lascano & Wilson 1978: b = 5·12). The saturated hydraulic conductivity (K_s, Eqn 5) was set to 11·1 mol s^{-1} MPa^{-1} m^{-1} based on data from van Bavel *et al*. (1978) and assuming their water content for a drained pot of 0·39 m height.

Vulnerability curve parameters c and d (Eqn 9) were the same as reported in Fig. 3 for water birch. In sunflower, they were obtained from the best fit of Eqn 9 to data obtained for mature stems (c = 3, d = 2·3; J. S. Sperry, unpublished results) using the centrifugal force method (Pockman *et al*. 1995; Alder *et al*. 1997). The sunflower vulnerability curve was very similar to that for boxelder stem xylem (Fig. 3).

Values for k_s of the plant elements (Eqn 9) were based on k measurements of root and shoot systems of well-watered plants using the vacuum canister method of Kolb, Sperry & Lamont (1996). This method gave approximate k_s values for the two root elements in series and the two shoot elements in series. Conductance was divided equally among the two elements within the root and shoot system.

The A_R:A_L was not measured. A range was estimated based on published values of root length per leaf area which range from 3900 to 14 000 m m^{-2} (Rendig & Taylor 1989). These correspond to A_R:A_L = 2·4–9·1, assuming r_s = 0·1 mm. Measurements of A_L and a soil volume of 0·014 m^3 allowed us to set a corresponding range of L (Table 4).

Given the uncertainty of A_R:A_L, and of using k_s values measured on nonintact plants to represent the *in situ* values, we used the model to estimate a liberal range of E_{crit} values as a function of soil Ψ (i.e. Ψ_{16}). The high end was based on maximum A_R:A_L in combination with a 20% increase in k_s of each plant element over the measured value; the low end used minimum A_R:A_L and a 20% decrease of k_s.

To obtain data on how E varied with soil Ψ (Ψ_s), water was withheld and periodic measurements of E and Ψ_s were made during the drought. The E was measured in a whole-canopy open gas exchange system as described in Saliendra *et al*. (1995). The E measurements were destructive because leaf area was measured by defoliating the plant and using a bench-top leaf area meter (LiCor, Lincoln, NE, USA). The Ψ_s was measured psychrometrically by removing soil samples from ports in the sides of the pots at 300 mm depth (n = 3 samples per pot) and sealing the samples in psychrometer chambers (Merrill Scientific, Logan, UT, USA).

RESULTS

Analysis of E_{crit} and Ψ_{crit}

The dependence of E_{crit} on Ψ_s is shown in Fig. 4 for loam soil (Table 2). The five xylem types are shown, four with varying cavitation resistance (open symbols) and one with no cavitation (solid symbols). Where the non-cavitating curve shows higher E_{crit} and lower Ψ_{crit} than the cavitating curves, the xylem was limiting. Where the two curves are the same, the rhizosphere was limiting. For all curves, E_{crit} decreased to zero as Ψ_s decreased to Ψ_{crit} (Ψ_{crit} is shown by arrows on the Ψ_s axis in Fig. 4a).

At the relatively high A_R:A_L of 10 in Fig. 4a, xylem cavitation was limiting (compare open versus solid symbols). The

	Sunflower		Water birch	
Parameter	measured	setting	measured	setting
Whole plant ks (mmol $s^{-1}MPa^{-1}$)	1·45 ± 0·77	1·45 ± 20%	2·18 ± 0·76	2·18 ± 20%
% R 3+4	85 ± 4	80	52 ± 8	50
A_L (m^2)	0·195 ± 0·119	0·195	0·321 ± 0·1	0·321
L (mm mm^{-3})	–	0·054–0·195	–	0·089–0·321

Table 4. Plant parameter settings for sunflower and water birch simulations shown in Fig. 8. Soil settings were for fritted clay (Table 2) using a soil volume of 0·014 m^3. Means are based on n = 10 plants for sunflower and n = 9 plants for water birch. Plant parameters were whole-plant k_s (all four elements in series), percentage of total resistance in elements 3 and 4 (% R 3+4, with equal resistances per element), leaf area (A_L) and root length density (L). Settings for L corresponded to a range of 2·4–9·1 forA_R/A_L. The d and c values for the Weibull function (Eqn 9) are given in Fig. 3 for water birch, and were 2·3 and 3, respectively, for sunflower

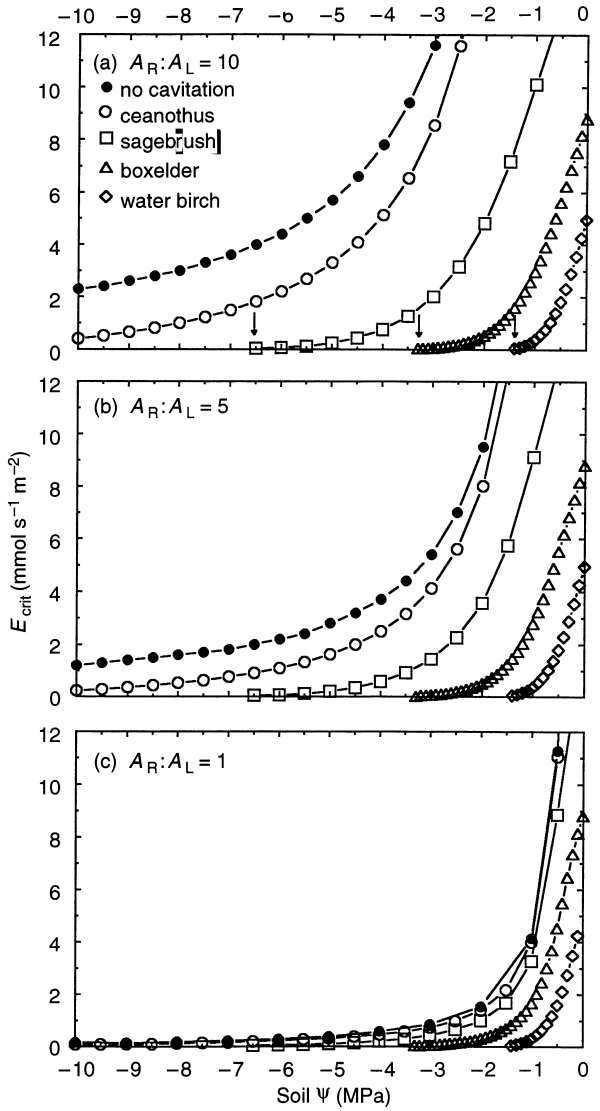

Figure 4. E_{crit} versus soil Ψ (Ψ_{16}) in loam soil (Table 2) at three different values of A_R:A_L (a – c). 'No cavitation' values (closed symbols) give E_{crit} as limited by rhizosphere conductance alone. Four types of cavitating xylem are based on the $k(\Psi)$ functions shown in Fig. 3. Arrows on the *x*-axis in (a) indicate Ψ_{crit}.

more vulnerable the xylem to cavitation, the lower was E_{crit} at a given Ψ_s, and the higher (less negative) was Ψ_{crit}. The Ψ_{crit} was sufficient to cause ≈ 98–99% loss of xylem conductance based on the xylem vulnerability curve (Fig. 3).

Decreasing A_R:A_L from 10 to 5 (Fig. 4b) and 1 (Fig. 4c) caused a gradual transition from xylem cavitation to rhizosphere conductance as the limiting factor for E_{crit} and Ψ_{crit}. This is evident from the identical E_{crit} for ceanothus xylem versus non-cavitating xylem at A_R:A_L = 1 (Fig. 4c). The same was nearly true for sagebrush. The more cavitation-susceptible xylem types (boxelder, water birch) were still xylem-limited (Fig. 4c). However, as A_R:A_L was decreased further (data not shown), the rhizosphere became limiting for all xylem types.

Figure 5 extends the findings in Fig. 4 to different soils. It shows Ψ_{crit} as a function of A_R:A_L for cavitating (solid lines) versus non-cavitating (dashed lines) xylem. Figure 5a is for sandy loam (Table 2). At lower A_R:A_L, the Ψ_{crit} was the same with or without cavitation (overlapping dashed and solid lines) and the rhizosphere was limiting. At higher A_R:A_L, the Ψ_{crit} for cavitating xylem converged on the Ψ causing 98–99% loss in xylem conductance (Fig. 3) while the Ψ_{crit} for non-cavitating xylem continued to decrease. The threshold A_R:A_L marking the transition between rhizosphere versus xylem limitation is where Ψ_{crit} values for cavitating versus non-cavitating xylem depart.

It is evident from Figs 4 and 5a that each xylem type had a threshold A_R:A_L above which xylem cavitation was limiting and below which the rhizosphere conductance was limiting. The A_R:A_L threshold increased as cavitation resistance increased.

Figure 5b generalizes the results in Fig. 5a across five soil types. The dashed lines again represent Ψ_{crit} in the absence of cavitation, with lines 1–5 indicating soils of

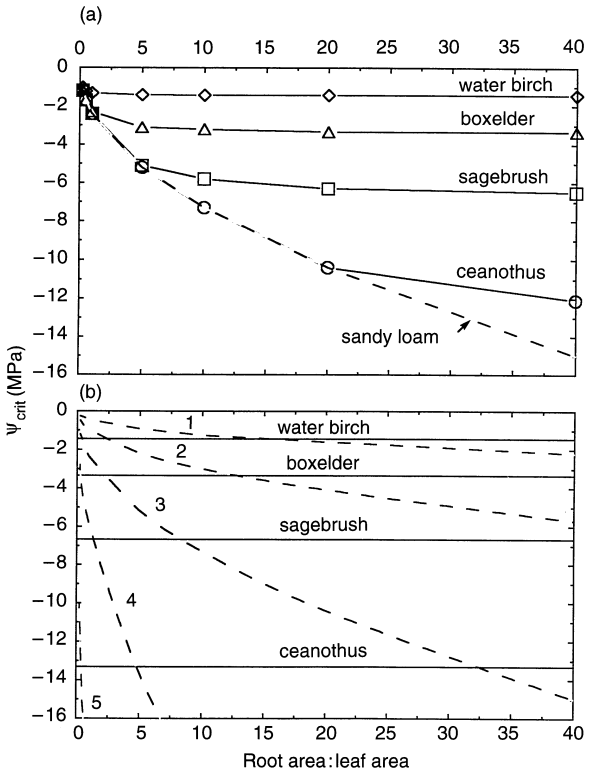

Figure 5. Ψ_{crit} versus A_R:A_L. (a) Sandy loam. The curved dashed line is for no cavitation where Ψ_{crit} was determined by rhizosphere hydraulics alone. Solid lines are for cavitating xylem of the indicated type. Where solid lines depart from the dashed line, xylem rather than rhizosphere becomes more limiting for plant fluxes and pressures. (b) Data for five soil types superimposed. Numbered dashed curves are for non-cavitating xylem in sand (1), loamy sand (2), sandy loam (3), silt loam (4), and loam (5). Horizontal solid lines are for cavitating xylem of the indicated type. The transition between soil versus xylem limitation of flux and pressure is approximated by the intersection of dashed and solid lines.

increasingly finer texture from sand to loam (3 is sandy loam from Fig. 5a). The horizontal solid lines represent $\Psi_{crit} = \Psi$ at 99% loss of xylem conductance. The A_R:A_L threshold for a given soil and xylem type is approximated by the intersection of dashed and solid lines. The actual transition was smooth (Fig. 5a) indicating a range of A_R:A_L over which the rhizosphere exerted a gradually diminishing influence (compare Figs 5a & b).

The coarser the soil type, the more limiting the soil was to plant fluxes and pressures relative to the xylem, and the higher was the A_R:A_L threshold for xylem limitation. For example, the coarsest soil (sand, dashed line 1), limited Ψ_{crit} in all but the most cavitation-susceptible type (water birch), and then only at the highest A_R:A_L. In contrast, in the finest soil analysed (loam, dashed line 5), the xylem determined Ψ_{crit} even in the most cavitation-resistant species. Simulations for soils finer than loam were all xylem-limited.

Increasing A_R:A_L above the xylem-limiting threshold continued to influence E_{crit} up to a second threshold (Fig. 6). The influence is evident in the sagebrush results in Fig. 4: increasing A_R:A_L caused E_{crit} to increase for intermediate Ψ_s (e.g. $\Psi_{crit} > \Psi_s < 0$). The E_{crit} was maximized by progressively higher A_R:A_L in more cavitation-resistant species (Fig. 6).

The results in Fig. 5 show conditions under which xylem versus rhizosphere conductance is more hydraulically limiting, but they do not indicate in which conducting element k approaches zero at hydraulic failure. When the xylem was limiting, the element with $k \cong 0$ was in the leaf element, because it has the lowest Ψ, and also in the transporting root element, if the root elements were more vulnerable to cavitation than the stem elements (as for water birch and boxelder). Figure 7 shows an example from boxelder xylem under xylem-limiting conditions (triangles, sandy loam soil, A_R:A_L = 27). The leaf and transporting root elements (1 and 3) had near-zero hydraulic conductance at E_{crit} (Fig. 7, solid triangles). Although a substantial reduction in hydraulic conductance also occurred at the root–soil interface, rhizosphere element conductance (e.g. 5, 6 and 7) was still above that in xylem elements 1 and 3. (Note: elements were exponentially shorter as they approached the root; Fig. 2).

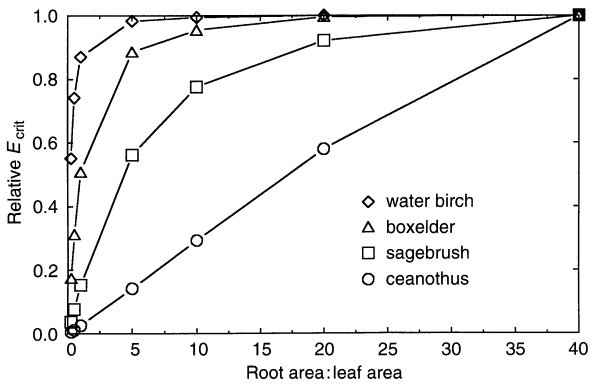

Figure 6. E_{crit} relative to E_{crit} at A_R:A_L = 40. All values are for loam soil at soil $\Psi = 1/3\ \Psi_{crit}$ (xylem-limiting conditions).

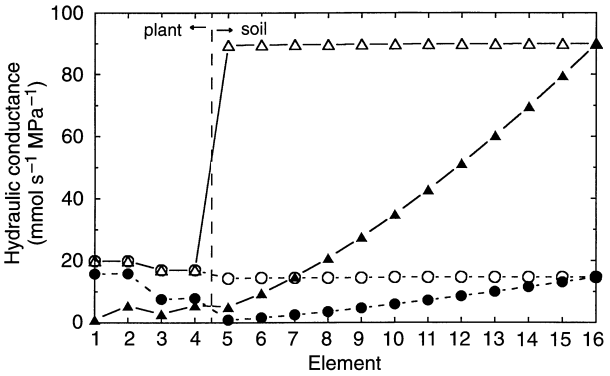

Figure 7. Hydraulic conductance of model elements (Fig. 2) for boxelder in sandy loam soil at $\Psi_{16} = -0{\cdot}5$ MPa. Element conductance is shown at $E = 0{\cdot}01$ mmol s^{-1} m^{-2} (open symbols = 'resting conductance') and at $E = E_{crit}$ (solid symbols) for a xylem-limiting A_R:A_L of 26·7 (triangles, solid lines) and a soil-limiting A_R:A_L of 1 (circles, dashed lines). The xylem limitation was evident from the near-zero hydraulic conductance in elements 1 and 3 at E_{crit} (solid triangles), and the soil limitation resulted from near-zero conductance in elements 5–7 (solid circles).

When the soil conductance was limiting E_{crit}, the hydraulic bottleneck at the root–soil interface was responsible. Figure 7 also shows boxelder under soil-limiting conditions (circles, sandy loam soil, A_R:A_L = 1). At E_{crit}, the elements with the lowest conductance were adjacent to the root surface (Fig. 7, solid circles, elements 5, 6 and 7) rather than in the plant.

It should be emphasized that, while E_{crit} and Ψ_{crit} are associated with k reaching zero somewhere in the continuum, the *total* conductance in the continuum may still be substantial. In Fig. 7, for example, the total loss of conductance in the continuum at E_{crit} was 58% and 86% for xylem- and rhizosphere-limited cases, respectively.

Decreasing A_R:A_L transferred the hydraulic limitation from xylem to rhizosphere because it reduced the 'resting' (i.e. E near 0) rhizosphere conductance (Fig. 7; compare open triangles with open circles), therefore causing the rhizosphere bottleneck to create the lowest k values in the continuum as E approached E_{crit}. At high A_R:A_L, the resting conductance in the rhizosphere was much greater than in the plant (Fig. 7, open triangles); thus, even though a rhizosphere bottleneck developed as E increased, it did not result in the limiting conductance for the continuum. Lower A_R:A_L brought the resting conductance closer to those in the plant (Fig. 7, open circles) with the result that rhizosphere conductance became limiting as flux increased. At intermediate A_R:A_L, the relative limitation of rhizosphere versus xylem was less pronounced, and both components exerted influence, as evidenced by the smooth transition from rhizosphere to xylem limits in Fig. 5a, and the influence of A_R:A_L on E_{crit} under xylem-limited conditions (Fig. 6).

Sensitivity analysis

Table 3 summarizes a sensitivity analysis for secondary model parameters under xylem-limited conditions. As

expected, $\Psi_{crit} = \Psi$ at 98–99% loss of xylem conductance regardless of parameter settings.

The E_{crit} increased 7·1% for a 40% increase in whole-plant k_s/A_L (maximum leaf-specific conductance). The effect of increasing L (and A_R) was primarily due to the increase in l (28·6% response) rather than a decrease in r_{max} (10·7% response), meaning that total root length was more important than density. The E_{crit} was not influenced by the allotment of k_s among elements; however, it did increase by 9·6% when the absorbing root k was held constant (Table 3).

The E_{crit} values were for steady-state conditions where Ψ of outermost soil node was held constant. As a result, capacitance had no influence on E_{crit} (Table 3). In reality, soil Ψ will decrease as water is withdrawn. However, when we modelled the non-steady-state case we found no significant change in the E_{crit} versus Ψ_s relationships shown in Fig. 4 (simulations not shown).

Controlled drought experiments

Figure 8 shows the comparison between model predictions of E_{crit} versus Ψ_s, and data from controlled drought experiments. A range of E_{crit} is shown based on a ±20% deviation in plant k_s from measured values and a 2·4–9·1 range in A_R:A_L (see Table 4 for parameters). Xylem cavitation was limiting for both sunflower and water birch. The greater resistance of sunflower to cavitation than water birch is reflected in the lower Ψ_{crit} and greater E_{crit} of sunflower than water birch (Fig. 8).

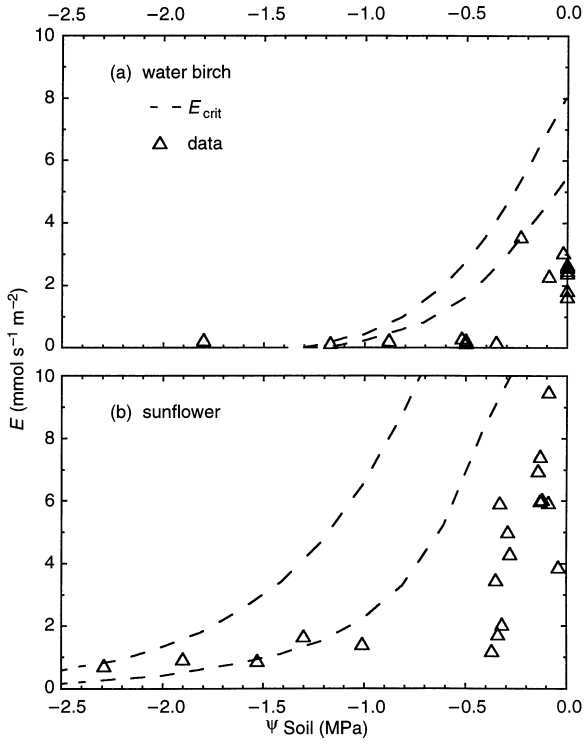

Figure 8. E versus soil Ψ for water birch (a) and sunflower (b). Dashed lines are maximum and minimum estimates of E_{crit} based on parameters in Table 4. Open triangles are data from controlled drought experiments.

In both species, stomatal closure during drought was necessary and sufficient to keep E below maximum E_{crit} and so avoid a predicted hydraulic failure. However, safety margins from the E_{crit} range decreased substantially as drought progressed. As predicted because of its greater cavitation resistance, sunflower maintained higher E relative to water birch at all soil Ψ. If water birch had not restricted E below that of sunflower, the model would predict hydraulic failure, even under well-watered conditions.

DISCUSSION

Both rhizosphere and xylem constraints were important for setting the range of possible flux and pressure in plants, but their relative importance depended on conditions. The rhizosphere was limiting for low A_R:A_L, coarse textured soils, and species resistant to cavitation. Xylem cavitation was limiting for higher A_R:A_L, fine textured soils, and species vulnerable to cavitation (Fig. 5b). The incorporation of the rhizosphere component is a significant improvement over previous attempts to estimate hydraulic limits (Tyree & Sperry 1988; Jones & Sutherland 1991; Alder *et al*. 1996).

The method of analysis also improves over earlier attempts. Previous models did not employ the Kirchhoff transform (Ross & Bristow 1990), and their accuracy depended on how finely the continuum was discretized (Appendix). Insufficient discretizing resulted in predictions of Ψ_{crit} much less negative than that which caused 100% loss of xylem conductance (Jones & Sutherland 1991; Alder *et al*. 1996; Mencuccini & Comstock 1997). While Jones & Sutherland (1991) emphasized that stomatal conductance may be maximized at the expense of some xylem conductance, our model predicts that stomatal conductance (a proxy of E) will be maximized at the expense of *all* conductance at the limiting point in the continuum. According to Fig. 7 this will be in the root and/or leaf xylem under xylem-limiting conditions, or in the rhizosphere. At E_{crit} the loss of conductance for the entire continuum (soil-to-leaf) may be substantially below 100% (e.g. 59–86% for simulations in Fig. 7).

Assuming a benefit from maximizing leaf area and stomatal conductance while minimizing root biomass and cavitation resistance, plants should operate as close as they can to their hydraulic limits without risking failure. This is consistent with the drought experiments (Fig. 8), and the analysis of Tyree & Sperry (1988). Although the Tyree & Sperry study did not incorporate the Kirchhoff transform or rhizosphere resistances, it was discretized and would match our model predictions under xylem-limiting conditions. A large body of empirical work also supports the existence of small safety margins in plants that are relatively vulnerable to cavitation and likely to be xylem-limited (Sperry & Pockman 1993; Sperry, Alder & Eastlack 1993; Tyree *et al*. 1993, 1994; Cochard *et al*.

1996; Saliendra *et al*. 1995; Alder *et al*. 1996; Lu *et al*. 1996).

Plants with very cavitation-resistant xylem (sagebrush, ceanothus) may only approach their hydraulic limits when Ψ_s drops during drought. At high Ψ_s, the E_{crit} for these xylem types (Fig. 4) was far above typical maximum values for plants (≈ 10 mmol s^{-1} m^{-2}), and E would probably be limited by other factors such as the maximum diffusive conductance of the leaf-to-water vapour. A decrease in Ψ_s during drought would reduce E_{crit} well within the physiological range and constrain gas exchange, a prediction borne out by application of the model to field data from sagebrush (Kolb & Sperry, manuscript in preparation) and ceanothus (Portwood *et al*. 1997).

Being able to predict hydraulic limitations based on interactions between soil type, water availability, A_R:A_L, and xylem type (Fig. 5b) leads naturally to hypotheses about adaptive combinations of these properties. A set of these hypotheses can be formulated if we assume at the outset that plants operate near their hydraulic limits, at least on a seasonal basis.

The most general hypothesis is that plants will be near the A_R:A_L threshold where xylem is limiting. The A_R:A_L should be at least as high as the threshold because this minimizes Ψ_{crit}. Increases in A_R:A_L beyond the threshold confer progressively diminishing returns with respect to water uptake (Figs 5 & 6), and would represent a waste of root biomass with respect to water uptake.

The evidence suggests that most plants are xylem-limited. Measurements of A_R:A_L vary tremendously, from 0·24 to over 10 (Tyree *et al*. 1998; Rendig & Taylor 1989). Even at the low end of this range, all plants would be xylem limited if growing in a loam- or finer-textured soil (Fig. 5b, dashed line 5). Excess of A_R:A_L beyond the threshold may reflect requirements for uptake of nutrients rather than water. For a modest A_R:A_L of 2, soils would have to be at least as coarse as a sandy loam (Fig. 5b, dashed line 3) to limit fluxes in relatively cavitation-susceptible plants such as boxelder, water birch, and probably most crop species (Sperry 1998). These conclusions are consistent with Newman's (1969) analysis of the rhizosphere bottleneck, wherein he estimated that, for a sandy loam, A_R:A_L less than 0·62 would be necessary for an appreciable rhizosphere resistance to develop. Our results also parallel those of Bristow *et al*. (1984) where rhizosphere resistances influenced plant water uptake for coarse soils with a b value below 3·5 (Table 2), and other factors constrained uptake in finer soils ($b > 3·5$).

A related hypothesis is that plants growing in drought-prone habitats should be more resistant to cavitation and have higher A_R:A_L than plants in wetter habitats. This is true with respect to cavitation resistance (Sperry 1998), and in many instances for root density (Glinski & Lipiec 1990) which may correspond to higher A_R:A_L.

Superimposed on the hypothetical trend with drought exposure are adaptive trends related to soil type. Plants should be hydraulically compatible with their soil. Plants in finer textured soils would tend to develop the lowest A_R:A_L and have the widest range of cavitation resistance. Plants in sandier soils would have the highest A_R:A_L and be more uniformly vulnerable to cavitation. Rooting density is known to be higher for certain plants in coarse versus fine soils (Glinksi & Lipiec 1990), and a recent analysis of vulnerability curves of forests in Brunei indicated rather uniformly vulnerable xylem for species of the heath and Dipterocarp forests on relatively coarse soil (Becker, Patino & Tyree 1998).

A caveat to these hypotheses is that an increase in E_{crit} and/or a decrease in Ψ_{crit} can have the disadvantage of promoting faster consumption of water and accelerating soil drought. This is the case where a fixed soil volume is available to the roots, as in potted plants. In the ground, however, the total soil volume drained by roots is more ambiguous, and could actually be dependent on the manner in which E is regulated during the drought. Drought simulations incorporating pararhizal resistances (Newman 1969) and larger soil volumes would be necessary to explore these interactions.

The use of the pipe model leads to an even draining of the soil volume and an even distribution of cavitation among morphologically equivalent units of the plant. This may approach reality for shallowly rooted plants with fibrous root systems and weak apical dominance in the shoot, but otherwise it is an oversimplification. Nevetheless, the prediction of Ψ_{crit} should not depend on the model's representation of hydraulic architecture because under xylem-limited circumstances it is constant at near the 100% loss point of the vulnerability curve (Table 3). The E_{crit}, however, may be more accurately predicted by a species-specific representation of morphology. The pipe model also predicts uniform hydraulic failure at E_{crit}, whereas the branched catena approach of Tyree & Sperry (1988) demonstrated a patchwork pattern of canopy dieback with hydraulically favoured branches surviving at the expense of others.

Synthesizing the effects of rhizosphere and xylem conductance on plant water use has led to explicit hypotheses concerning the coordinated evolution of root-shoot ratios and cavitation resistance in response to soil type and water availability. Evaluation of these hypotheses should be accompanied by finer resolution of the $k(\Psi)$ relationships in xylem of different organs (especially roots and leaves), and in non-xylary tissues of roots and leaves, as well as a more quantitative understanding of root architecture and function.

ACKNOWLEDGMENTS

This work was supported by NSF (IBN-9319180) and USDA (9500965) grants to J.S.S. N. Z. Saliendra conducted the controlled drought experiments in context of an associated project. We thank J.B. Passioura and W.T. Pockman for helpful discussions regarding preliminary versions of the model. The comments of three anonymous reviewers were useful in improving the manuscript.

REFERENCES

Alder N.N., Pockman W.T., Sperry J.S. & Nuismer S. (1997) Use of centrifugal force in the study of xylem cavitation. *Journal of Experimental Botany* **48,** 665–674.

Alder N.N., Sperry J.S. & Pockman W.T. (1996) Root and stem xylem embolism, stomatal conductance, and leaf turgor in *Acer grandidentatum* populations along a soil moisture gradient. *Oecologia* **105,** 293–301.

van Bavel C.H.M., Lascano R. & Wilson D.R. (1978) Water relations of fritted clay. *Soil Science Society of America Journal* **42,** 657–659.

Becker P., Patino S. & Tyree M.T. (1998) Vulnerability to drought-induced embolism of Bornean heath and dipterocarp forest trees. *Tree Physiology*.

Bristow K.L., Campbell G.S. & Calissendorff C. (1984) The effects of texture on the resistance to water movement within the rhizosphere. *Soil Science Society of America Journal* **48,** 266–270.

Caldwell M.M. & Richards J.H. (1986) Competing root systems: morphology and models of absorption. In *On the Economy of Plant Form and Function* (ed. T.J. Givnish), pp. 251–274. Cambridge University Press, Cambridge.

Campbell G.S. (1985) *Soil Physics with Basic; Transport Models for Soil-Plant Systems*. Elsevier Science Publishers, Amsterdam.

Cochard H., Breda N. & Granier A. (1996) Whole tree hydraulic conductance and water loss regulation in *Quercus* during drought: evidence for stomatal control of embolism? *Annales des Sciences Forestieres* **53,** 197–206.

Cochard H., Cruiziat P. & Tyree M.T. (1992) Use of positive pressures to establish vulnerability curves: further support for the air-seeding hypothesis and implications for pressure-volume analysis. *Plant Physiology* **100,** 205–209.

Cowan I.R. (1965) Transport of water in the soil-plant-atmosphere system. *Journal of Applied Ecology* **2,** 221–239.

Givnish T.J. (1995) Plant stems: biomechanical adaptation for energy capture and influence on species distributions. In *Plant Stems: Physiology and Functional Morphology* (ed. B.L. Gartner), pp. 3–49. Academic Press, San Diego.

Glinski J. & Lipiec J. (1990) *Soil Physical Conditions and Plant Roots*. CRC Press, Boca Raton.

Hacke U. & Sauter J.J. (1996) Drought-induced xylem dysfunction in petioles, branches and roots of *Populus balsamifera* L. & *Alnus glutinosa* (L) Gaertn. *Plant Physiology* **100,** 1020–1028.

Hellkvist J., Richards G.P. & Jarvis P.G. (1974) Vertical gradients of water potential and tissue water relations in Sitka spruce trees measured with the pressure chamber. *Journal of Applied Ecology* **7,** 637–667.

Hillel D. (1980) *Fundamentals of Soil Physics*. Academic Press, NY.

Jones H.G. & Sutherland R.A. (1991) Stomatal control of xylem embolism. *Plant Cell and Environment* **18,** 189–196.

Kolb K.J. & Sperry J.S. & Lamont B.B. (1996) A method for measuring xylem hydraulic conductance and embolism in entire root and shoot systems. *Journal of Experimental Botany* **47,** 1805–1810.

Landsberg J.J., Blanchard T.W. & Warrit B. (1976) Studies on the movement of water through apple trees. *Journal of Experimental Botany* **27,** 579–596.

Lopez F.B. & Nobel P.S. (1991) Root hydraulic conductivity of two cactus species in relation to root age, temperature, and soil water status. *Journal of Experimental Botany* **42,** 143–150.

Lu P., Biron P., Granier A. & and Cochard H. (1996) Water relations of adult Norway spruce (*Picea abies* (L) Karst) under soil drought in the Vosges mountains: whole-tree hydraulic conductance, xylem embolism and water loss regulation. *Annales des Sciences Forestieres* **53,** 113–121.

Meinzer F.C., Goldstein G., Jackson P., Holbrook N.M., Gutierrez M.V. & Cavelier J. (1995) Environmental and physiological regulation of transpiration in tropical forest gap species: the influence of boundary layer and hydraulic conductance properties. *Oceologia* **101,** 514–522.

Meinzer F.C., Goldstein G., Neufeld H.S., Grantz D.A. & Crisosto G.M. (1992) Hydraulic architecture of sugarcane in relation to patterns of water use during development. *Plant Cell and Environment* **15,** 471–477.

Mencuccini M. & Comstock J.C. (1997) Vulnerability to cavitation in populations of two desert species, *Hymenoclea salsola* and *Ambrosia dumosa*, from different climatic regions. *Journal of Experimental Botany* **48,** 1323–1334.

Neufeld H.S., Grantz D.A., Meinzer F.C., Goldstein G., Crisosto G.M. & Crisosto C. (1992) Genotypic variability in vulnerability of leaf xylem to cavitation in water-stressed and well-irrigated sugarcane. *Plant Physiology* **100,** 1020–1028.

Newman E.I. (1969) Resistance to water flow in soil and plant. I. Soil resistance in relation to amounts of root: theoretical estimates. *Journal of Applied Ecology* **6,** 1–12.

Passioura J.B. & Cowan I.R. (1968) On solving the non-linear diffusion equation for the radial flow of water to roots. *Agricultural Meteorology* **5,** 129–134.

Pockman W.T., Sperry J.S. & O'Leary J.W. (1995) Evidence for sustained and significant negative pressure in xylem. *Nature* **378,** 715–716.

Portwood K.A., Ewers F.W., Davis S.D., Sperry J.S. & Adams C.G. (1997) Shoot dieback in Ceanothus chaparral during prolonged drought – a possible case of catastrophic xylem cavitation. *Bulletin Ecological Society of America.* **78,** 298.

Press W.H., Flannery B.P., Teukolsky S.A. & Vetterling W.T. (1989) *Numerical Recipes in Pascal; The Art of Scientific Computing*. Cambridge University Press, Cambridge.

Rawlings J.O. & Cure W.W. (1985) The Weibull function as a dose–response model to describe ozone effects on crop yields. *Crop Science* **25,** 807–812.

Rendig V.V. & Taylor H.M. (1989) *Principles of Soil-Plant Interrelationships*. McGraw Hill, New York.

Ross P.J. & Bristow K.L. (1990) Simulating water movement in layered and gradational soils using the Kirchhoff transform. *Soil Science Society of America Journal* **54,** 1519–1524.

Saliendra N.Z. & Meinzer F.C. (1989) Relationship between root/soil hydraulic properties and stomatal behavior in sugarcane. *Australian Journal of Plant Physiology* **16,** 241–250.

Saliendra N.Z., Sperry J.S. & Comstock J.P. (1995) Influence of leaf water status on stomatal response to humidity, hydraulic conductance, and soil drought in *Betula occidentalis*. *Planta* **196,** 357–366.

Shinozaki K., Yoda K., Hozumi K. & Kira T. (1964) A quantitative analysis of plant form – the pipe model theory. I. Basic analyses. *Japanese Journal of Ecology* **14,** 97–105.

Sperry J.S. (1998) Hydraulic constraints on plant gas exchange. *Agricultural and Forest Meteorology*, in press.

Sperry J.S., Alder N.N. & Eastlack S.E. (1993) The effect of reduced hydraulic conductance on stomatal conductance and xylem cavitation. *Journal of Experimental Botany* **44,** 1075–1082.

Sperry J.S. & Pockman W.T. (1993) Limitation of transpiration by hydraulic conductance and xylem cavitation in *Betula occidentalis*. *Plant, Cell and Environment* **16,** 279–288.

Sperry J.S. & Saliendra N.Z. (1994) Intra- and inter-plant variation in xylem cavitation in *Betula occidentalis*. *Plant, Cell and Environment* **11,** 35–40.

Steudle E. (1994) The regulation of plant water at the cell, tissue, and organ level: role of active process and of compartmentation. In *Flux Control in Biological Systems. From Enzymes to Populations and Ecosystems* (ed. E.D. Schulze), pp. 237–299. Academic Press, San Diego.

Tyree M.T., Cochard H., Cruiziat P., Sinclair B. & Ameglio T. (1993) Drought induced leaf shedding in walnut: evidence for vulnerability segmentation. *Plant, Cell and Environment* **16,** 879–882.

Tyree M.T., Kolb K.J., Rood S.B. & Patino S. (1994) Vulnerability to drought-induced cavitation of riparian cottonwoods in Alberta: a possible factor in the decline of the ecosystem? *Tree Physiology* **14,** 455–466.

Tyree M.T. & Sperry J.S. (1988) Do woody plants operate near the point of catastrophic xylem dysfunction caused by dynamic water stress? Answers from a model. *Plant Physiology* **88,** 574–580.

Tyree M.T., Velez V. & Dalling J.W. (1998) Root and shoot hydraulic growth dynamics in five neotropical seedlings of differing light requirements: scaling to show ecotype differences. *Oecologia*, in press.

Yang S. & Tyree M.T. (1993) Hydraulic resistance in *Acer saccharum* shoots and its influence on leaf water potential and transpiration. *Tree Physiology* **12,** 231–242.

Yang S. & Tyree M.T. (1994) Hydraulic architecture of *Acer saccharum* and *A. rubrum*: comparison of branches to whole trees and the contribution of leaves to hydraulic resistance. *Journal of Experimental Botany* **45,** 179–186.

Zimmermann M.H. (1983) *Xylem Structure and the Ascent of Sap*. Springer, Berlin.

Received 20 August 1997; received in revised form 12 January 1998; accepted for publication 13 January 1998

APPENDIX

Solution of E_{crit} and Ψ_{crit}

Equation 1, Darcy's law, can be expressed in terms of hydraulic conductance between two points in the flow path, where $k(\Psi)$ represents the Ψ-dependent leaf-specific hydraulic conductance between those points:

$$E = -k(\Psi)\, x_l\, d\Psi/dx, \quad \text{(A1)}$$

where x_l is the distance between the points. If $k(\Psi)$ represents the conductance between soil and leaf, Eqn A1 can be solved for E_{crit} by separating variables and integrating over the soil–leaf continuum, yielding:

$$E = -\int_{\Psi_s}^{\Psi_l} k(\Psi)\, d\Psi, \quad \text{(A2)}$$

where Ψ_l = leaf Ψ and Ψ_s = soil Ψ. E is maximized (= E_{crit}) when $\Psi_l = \Psi_{crit}$ = limit of Ψ as k goes to zero. The Ψ_{crit} is independent of Ψ_s, and E_{crit} decreases as Ψ_s decreases.

The Kirchhoff transform and the solution of E_{crit} and Ψ_{crit}

Transforming Eqn A1 in terms of matric flux potential (Φ) equates to:

$$E = -x_l\, d\Phi/dx. \quad \text{(A3)}$$

Separating variables and integrating over the continuum from soil to leaf (as for Darcy's law, above) gives:

$$E = -(\Phi_L - \Phi_S), \quad \text{(A4)}$$

where Φ_L and Φ_S represent leaf and soil Φ, respectively. From the definition of Φ in Eqn 10:

$$(\Phi_L - \Phi_S) = \int_{\Psi_s}^{\Psi_l} k(\Psi)\, d\Psi. \quad \text{(A5)}$$

Substituting E for $-(\Phi_L - \Phi_S)$ in Eqn A5 gives Eqn A2 as derived from Darcy's law. $E = E_{crit}$ under the same conditions as for Eqn A2.

The use of matric flux potential for a single element model (i.e. two nodes, soil and leaf) yields the correct value for steady-state E_{crit} and Ψ_{crit} as long as the $k(\Psi)$ function is identical throughout the pathway. Discretizing is only necessary when there is a change in the $k(\Psi)$ function. In contrast, numerically solving Darcy's law for the same parameters requires extensive discretizing even if the $k(\Psi)$ function is constant in the continuum. For example, assuming a linear $k(\Psi)$ function with a zero intercept, no discretizing caused a 50% underestimation of E_{crit} and overestimation of Ψ_{crit}. Over 30 elements were required to get within 5% of the correct values.